Proceeding of the 13th National Mechanical Engineering Conference
2-3 December 1999, Royal Cliff Beach Resort Hotel, South Pattaya, Cholburi

Effect of End-Wall Opening on Temperature Distribution in A Ventilated Chamber

Chompicha Khuhiran, Jittima Mantajit, Saensuk Wetchagarun, Sasirat Boonrat, Thaworn Katsuwon, Tosapole Stitsuwongkul and Asi Bunyajitradulya

Fluid Mechanics Research Laboratory, Department of Mechanical Engineering,
Faculty of Engineering, Chulalongkorn University,
Bangkok 10330, Thailand
Tel. 218-6645, 218-6647; Fax. 252-2889; E-mail basi@chula.ac.th

Abstract

Effect of the size of end-wall opening t on temperature distribution in a ventilated chamber was investigated. The chamber had a dimension of 50x50x100 cm^3 (WxHxL) with a supply-air inlet of 4x50 cm^2 at the top of one end wall and an adjustable-opening discharge at the bottom of the other. Heated air was supplied at the inlet and the temperature distribution inside the chamber was measured for various widths of the opening, ranging from fully open to almost fully closed. The results showed that the characteristics of the distribution of temperature in the chamber depends on the relative size of the closing width s ($=H-t$) and the (otherwise) width or thickness of the wall jet δ on the ceiling at the discharge plane of a fully open case. Specifically, change in the closing width s has significant impact on the characteristics of the distribution of temperature only in the regime of $s <\sim \delta$. In the other regime, i.e., $s > \delta$, it has almost no effect on the distribution of temperature in the chamber. This result has significant implication and application in terms of flow control in a ventilated chamber.

1. Introduction

Ventilation in a chamber is a subject of many technological applications, the most obvious being in a ventilated/air-conditioned room. However, other applications include those in a combustion chamber, in a storage room, in a stir tank, etc.

This study is part of the FMRL's research program on flow control/manipulation for the enhancement of mixing in a mixing or ventilated chamber. The subject at hand is the effect of the size of end-wall opening, or closing, on the flow pattern in the chamber. Specifically, the effect of the size of the opening on the distribution of passive scalars like temperature is aimed. The premise is that if the characteristics of the flow in a chamber for various flow configurations is understood, means can be invented to manipulate or control the flow in order to achieve a desired effect at the most suitable parameters and ranges of these parameters.

The flow configuration chosen in this study is that of a chamber with an inlet on one end wall and an exit on the opposite. The chamber is supplied with heated air at the inlet and the temperature distributions in the chamber are measured for various sizes of opening.

Similar studies can be found from Nielsen et al. (1978), Gosman et al. (1980), and Peng et al. (1997). These studies, however, gave no indication of the effect of the size of end-wall opening, either on the velocity field or passive scalar field.

2. Experimental setup

The experiments were conducted in the Fluid Mechanics Research Laboratory (FMRL), Department of Mechanical Engineering, Faculty of Engineering, Chulalongkorn University. Figure 1 shows the schematic of the flow facility. The facility is basically a blower tunnel with heaters installed. Room air is drawn into the facility by a 3-hp centrifugal blower. At the exit of the blower, which is 3 inches in diameter, is a flexible duct employed in order to isolate vibration from the blower to the rest of the test rig. Air from the duct is discharged into a 50x50 cm^2 chamber. In the chamber, three mesh-4 screens are used to disperse the jet-like flow from the duct so that the flow fills the chamber, or becomes more uniform. In addition, they are used to generate high level of freestream turbulence so that the heaters are operated efficiently. In short, it is preferable to have uniform flow with high level of freestream turbulence passing through the heaters for efficient heat transfer. In the heating section, four 1.5-kw finned heaters are used for heating the air. To be able to adjust the air temperature, a 10 kVA variac is employed. Heated air from the heating section is then passed through the settling chamber section so that it can be conditioned for uniformity and low-turbulence level. The components in the settling chamber, from upstream to downstream, are a honeycomb made from 18-mm OD, 17-mm ID, 150-mm long brass tubes and

sandwiched between two mesh-16 screens, a series of four mesh-16 screens, and a mesh-30 screen; all are uniformly spaced at a distance of 150 mm. At the end of the settling chamber is a two-dimensional 12.5:1 contraction. The contraction exit is 50x4 cm^2 in size.

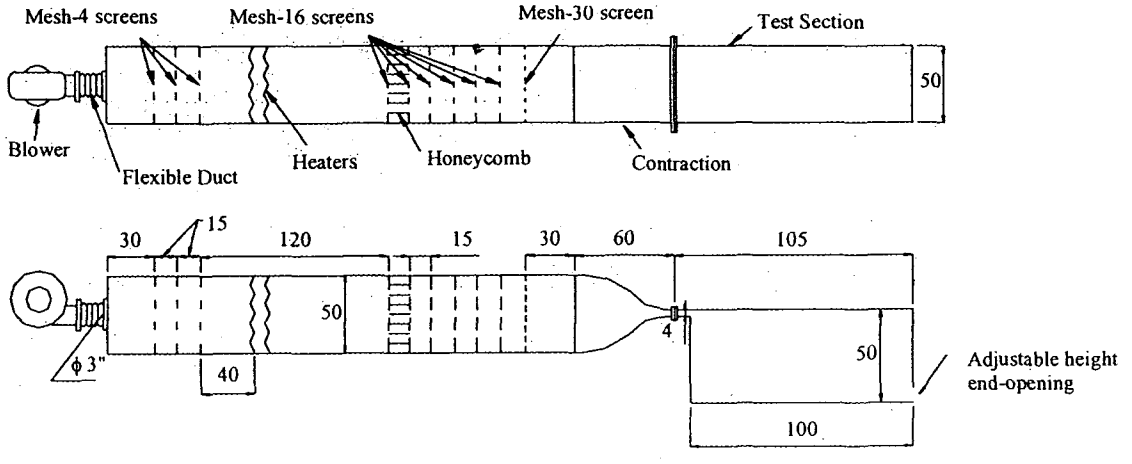

Fig. 1. Schematic of the flow facility; top – top view, bottom – side view. All dimensions are in cm unless specified.

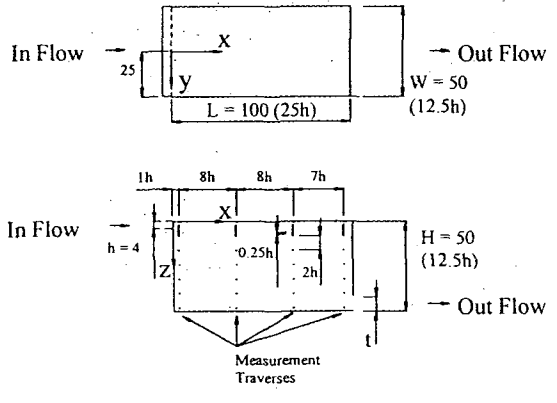

Fig. 2. Ventilated chamber. All dimensions are in cm unless specified.

Calibration of the flow facility, with the ventilated chamber removed, at a nominal speed of 7.9 m/s, and at a spatial resolution of 5cm x 1cm, showed practically uniform flow at the contraction exit. The boundary layer thicknesses, measured with the probe described in the companion paper by Sakulyanontvittaya et al. (1999) at three locations - one at the center and two on the sides - on each of the two wider walls were found to be less than 2mm.

Figure 2 shows the schematic of the ventilated chamber. The chamber is 50x50x100 cm^3 (WxHxL: W/H=1, L/H=2) in size and is made from acrylic plate of 5 mm thick. The inlet, which is 4 cm in height (h, h/H=0.08) - matched to the size of the contraction exit, is at the top and spans the whole width of the chamber. The end wall of the chamber is of adjustable height such that the height t of the end-opening can be varied.

Flow diagnostics include flow visualizations by tuft grid and by injection of powder, with an SLR- as well as a video-camera, and measurements of temperature distribution. The tuft grid used is similar to that described in the companion paper by Sathapornnanon et al. (1999). The injection of powder is achieved via a syringe and a hypodermic needle. The point of injection is at the mid-span of the inlet. Measurements of temperature are by means of a calibrated thermocouple with an accuracy of $\pm$ 1 °C and a thermometer.

Figure 2 shows the coordinates system employed as well as the spatial resolution for the measurements of temperature. Note that the origin of the coordinates system is on the upper wall and at the mid-span of the inlet of the chamber. Measurements of temperature are done on three traverse planes: the center plane (y=0 or y/W=0) and the planes y = $\pm$ 10.5 cm (y/W = $\pm$0.21). On each plane, four traverses in the z-direction, at x/L = 0.04, 0.36, 0.68, and 0.96, are performed. On each traverse, the spatial resolutions generally are 0.25h for $0<z<2h$ and 2h for $2h<z<H$.

A total of seven cases of different end-opening sizes, t, were tested: fully open, and 11.5-, 10.5-, 9.5-, 6.25- (half open), 2-, and 1-h openings. These correspond to t/H=1, 0.92, 0.84, 0.76, 0.5, 0.16, and 0.08, respectively. Note that cases 9.5h, 10.5h and 11.5h opening correspond to 3h, 2h and 1h closing, respectively. For convenience, we shall designate these cases as P1.0 (fully open), P0.92 (1h-closing), P0.84 (2h-closing), P0.76 (3h-closing), P0.5 (half open), P0.16 (2h-opening), and P0.08 (1h-opening), respectively. The tests were performed at the exit speed of 4.4 m/s, corresponding to Reynolds number based on h of approximately 10,000.

In all cases the temperatures of heated air at the chamber inlet, T_J, were approximately 69-74 °C, slightly

changed from case to case but stayed within ±0.5 °C in any one case. The room temperatures, T_R, during the experiment were within 30-32 °C, similarly stayed within ± 0.5 °C in any one case. And, the differences between the jet and the room temperatures were within 39-43 °C. Table 1 below gives details of these parameters.

Table 1. Inlet air and room temperatures in Celcius.

Case	P1.0	P0.92	P0.84	P0.76
T_J	71	72	70	71
T_R	30	31	30	31.5
Case	P0.5	P0.16	P0.08	
T_J	69	71	74	
T_R	30.5	30.5	31.5	

Finally, the results shall be presented in terms of the temperature coefficient C_T, defined as

$$C_T = \frac{T - T_R}{T_J - T_R},$$

where T is temperature at the measurement location.

3. Results

Flow visualization

Figure 3 (see back) shows examples of tuft-grid visualization images. In this case, they are of cases P1.0, P0.76, and P0.08. In these figures the flow is from right to left and the chamber inlet is at the top-right corner. In taking these images, an SLR camera was used with equal shutter speed of 8 sec. The reason for using long shutter speed is that we wanted to get some sense of *mean* flow direction. By using long shutter speed, the motion of tufts is recorded over a period of time such that motion-blur images result. Therefore, the direction and the angle in which the tufts sweep are approximately indicative of the mean flow direction and, to some extent, the unsteadiness of the flow at that point, albeit the error due to the weight of the tufts and flutter.

Figure 3a shows the result for case P1.0, a full opening. In effect, this is the case of a wall jet. As is apparent from the image, the tufts in the two top rows point towards the left while the rest, which are the majority, point slightly towards the right. The two top rows thus indicate the extent or the width of the jet. Since the tufts are spaced at approximately $1h$ apart in the vertical direction, this roughly indicates that the jet is 2 to $3h$ wide at the exit of the chamber. This shall be confirmed by the powder-injection image. In addition, the fact that the rest of the tufts - which are below the two top rows - point in the opposite direction, i.e., slightly towards the right indicates that there is some slight reverse flow *into* the chamber. One might be surprised at first but quickly then realizes that this is simply due to outside air flowing in as a result of the entrainment of inside air – which is flowing out - by the jet.

Figure 3b shows the result for case P0.76. Some differences from that of the former case are observed. Firstly, more tufts in the second and the third row from the top are now pointing towards the left, especially those in the middle and the left columns. If we trace the directions of the tufts from the inlet of the chamber, we may roughly see the trajectory and the extent of the jet. And, it appears that the jet from the inlet is deflected more downwards early on in the middle of the chamber and its extent grows more rapidly in the downstream direction, upto approximately $4h$ in width at the location of the second column from the left. Secondly, the tufts at the bottom rows are now pointing more towards the right. This indicates a stronger (and almost parallel) reverse flow near the bottom of the chamber in comparison with the former case. Thirdly, there is a region of relatively strong unsteadiness (temporally as well as directionally) under the inlet. This seems to indicate the region at which the reverse flow at the bottom, which is rising upwards, crashes with the jet stream from the inlet. Very similar patterns described above are also observed in case P0.08 in Fig. 3c.

Different perspective is given by the powder-injection images in Fig. 4, with tufts still in place. Note that these images are acquired through a video camera and frame-captured by an AGP card. Therefore, the exposure time is short and the tufts, unlike those in Fig. 3, are seen without motion blur. The dark stripe that cuts across the jet in all these images is due to obstruction in lighting. Of particular interest is the width of the jet δ at the chamber exit in case P1.0 (fully-open). It is observed to be approximately 2 to $3h$ wide, in accordance with that observed from tuft-grid method. In addition, the deflection of the jet downwards and the growth in width of the jet at downstream location in comparison with case P1.0 are observed in cases P0.76 and P0.08. Furthermore, reverse and recirculating flows of jet fluid (as opposed to outside air) are also observed in cases P0.76 and P0.08.

Temperature distribution

We shall first make comparisons of temperature distributions between various cases, then present some specific details of some of the cases for the reason that will soon become clear.

Figure 5 shows the temperature distributions, in the form of C_T, on the center plane (y=0) for four downstream locations. The uncertainty in the measurement of C_T is estimated to be within ± 0.07 for all cases. Figure 5a shows the distributions along the height of the room (z/H) at the location x/L=0.04, $1h$ downstream of the inlet of the chamber. The most striking features in this figure are the thin layers of high peaks near the upper wall (z/H=0) and the relatively uniform temperature region below these layers. The layers are approximately $0.2H$, or $2.5h$, wide. A closer look at the peaks indicates that they have values between 0.9-1.0 for all cases. Further examination shows that, as the end-opening width t decreases slightly from $1H$ (fully

open) to 0.76*H* (3*h* closing, or 1/4*H* closing), the level of temperature in the uniform region changes very rapidly - from approximately 0 in case P1.0 to 0.7 in case P0.76. In a striking contrast, after that even if the end-opening width decreases dramatically by a factor of almost 3/4*H* from case P0.76 to P0.08, the level of uniform temperature changes quite slowly or relatively remains constant at 0.7-0.8. This trend in change of the level of uniform temperature is similarly observed for all other downstream locations, upto the location near the chamber exit as illustrated in Figs. 5b-5d. This raises an interesting question of what happens to the flow in the regime of fully open to 1/4*H* closing (from case P1.0 to case P0.76) such that the characteristics of the flow changes drastically. A point we shall return in the next section.

A quick glance from top to bottom of Fig. 5 (from 5a to 5d), i.e., from upstream to downstream, shows that little change in temperature distribution and temperature level occurs in cases P0.5 to P0.08. Some exceptions are the decay of the peaks and, of particular interest, the development of the dip in temperature levels at mid height (of the chamber) as the flow evolves downstream. The latter, i.e., the dip, is even more pronounced in case P0.84, a 2*h* closing. Again, we shall come back to this point in the next section.

Since drastic change occurs in the regime from fully open to 1/4*H* closing, we present the corresponding cases together with case P0.5 for comparison in Fig. 6. Case P1.0, Fig. 6a, is a fully open case. The flow, in effect, as mentioned above is a wall jet whose width at the chamber exit is approximately 2 to 3*h*. From the figure, the thin layer of high peak is observed. And, as the flow evolves downstream, the extent of the layer grows and the peak decays, the characteristics of a wall jet. The peak is observed to decay from approximately 1 at x/L = 0.04 (inlet) to 0.5 at x/L = 0.96 (exit). Note that in this case, the wall jet is present, as the tuft-grid image (Fig. 3a) shows, with a counter-current stream of outside air created by the entrainment of the jet itself.

Figure 6b shows the distributions for case P0.92 (1*h* closing). In comparison to the former case, the characteristics of a wall jet is still observed from inlet upto x/L = 0.36. Further downstream, however, some deviation from a normal wall jet starts to appear at x/L = 0.68 and is pronounced at x/L = 0.96. Specifically, the jet grows rapidly. This is owing to adverse pressure gradient and, as a result, a deflection of the jet caused by the end wall.

The effect of the end wall becomes more pronounced in case P0.84, a 2*h* closing. The dip in temperature at mid height at x/L = 0.68 is obvious. From a different but related perspective, one may say that there is an abrupt increase in temperature from approximately constant at 0.5 in the upstream region of x/L = 0.68 to 0.65 as the flow evolves downstream to x/L = 0.96. Case P0.5 (Fig. 6d) and beyond, however, shows relatively uniform and similar temperature distribution throughout the chamber.

A quick glance from top to bottom of Fig. 6 (from 6a to 6d), i.e., from fully-opened to half-opened end wall, shows the effect of end-wall opening. At fully open, the temperature in the most part of the chamber is low, except the peak near the ceiling. As the end-wall opening decreases, the temperature in the room rises, being not so uniform at small closing but soon rapidly becomes uniform before half closing (Case P0.76).

Figure 7 shows the effect of end-wall opening on the maximum temperature, $C_{T\max}$, along the traverses. As the figure shows and as is to be expected, end-wall opening has the most impact at downstream location near the exit (large x/L) and has almost no effect at the upstream location near the inlet (small x/L). In addition, the figure also shows clearly that end-wall opening has the most impact on the flow in the range of $t/H > 0.75$-0.8. Below that, it has little impact irrespective of the location in the chamber.

To assess the two-dimensionality in the *mean* sense of temperature distribution in the chamber, preliminarily, the temperature distributions along two other spanwise planes, y = +10.5 and −10.5 cm, of selected cases were measured, and the result for case P0.92 is shown in Fig. 8. Although these two planes may not be close to the side walls enough, the volume between them accounts for 40% of the total volume of the chamber. And, it can give rough indication of the state of the flow in the chamber. In addition, because of the two dimensionality of the inlet (the inlet spans the whole width of the chamber), drastic deviation of temperature distribution from that of the center plane is not expected for at least 70% of the centered volume. The deviation is expected, however, in the region close to the side walls where boundary layers, thick or thin, are present. And, the reason for selecting case P0.92 is that it has the most highly non-uniform measured temperature distribution on the center plane. Thus, conceivably it is the most likely prone to non-uniformity in the spanwise direction. The result, shown in Fig. 8, indicates that the temperature distribution is fairly two dimensional, with some slight deviation at x/L = 0.36.

4. Discussion

Some interesting points arise from the study. Firstly, the observed rapid change in the characteristics of temperature distribution in the regime of the end-wall opening from fully-open to 1/4*H* closing and the dramatic contrast of relatively slow or no change in the rest of the regime, i.e., from 1/4*H* closing to almost fully closed, deserve some attention. Such change in characteristics most likely implies significant, if not drastic, change in the characteristics of the flow (in the chamber) in the former regime. Careful examination should reveal that this change in characteristics is related to the relative size of the width of the wall jet (case P1.0) at the exit of the chamber δ and the amount of end wall closing, $s=H-t$. Here, we offer some explanations. Starting from case P1.0, a fully open case, the flow exhibits the characteristics of a wall jet which has the width of approximately 2-3*h* at the exit of the chamber, an image presented (Figs. 3a and 4a) and a point discussed in the

last section. As the end wall is closed down by $1h$ (P0.92), which is smaller than the nominal width of the jet at that point, part of the wall jet is blocked from being normally discharged to outside and the jet is deflected downwards (see similar scenario in Fig. 3b) in the same manner as flow over a wall. The deflection of the jet results in an adverse pressure gradient in the streamwise direction which, in turn, causes a rapid growth of the jet in comparison with the simple wall jet of case P1.0. This results in an increase in temperature near the upper wall, especially at x/L = 0.96 and 0.68. Most of the mass of the *jet fluid*, we anticipate, still can go over the step and be discharged to outside, nonetheless, and no significant amount of the jet fluid is injected back into the chamber. The latter point concerning the amount of jet fluid being injected back into the chamber is drawn from the fact that there is no dip in the temperature profile (or, in other words, there is no region of high temperature near the bottom wall) at x/L = 0.36 and 0.68 in case P0.92 in comparison to cases P0.84 and beyond, a point which we shall reason below.

As the end wall is closed down further by $2h$ (P0.84), the size of which is comparable to the nominal width of the jet at that point, the jet is strongly and almost vertically deflected downwards such that the jet stream hits the bottom wall. As a result, the wall jet now changes its characteristics as it leaves the surface of an end wall to that of an impinging jet (impinge on the bottom wall) near the exit. And, as a consequence, some amount of jet fluid is now being injected back into the chamber as the jet impinges on the bottom wall. This, in turn, creates another layer of wall jet on the bottom wall and results in a region of high temperature near the bottom wall. The temperature profile particularly at x/L = 0.68, therefore, appears to have a dip in the middle. The reason that there is no dip in the profile at x/L = 0.96 is simply that this region is, more or less, well into the core of the impinging jet (the location is near the exit of the chamber). Thus, it has relatively high temperature and, as a result, no dip is observed.

Because of the region of high temperature created by the wall jet on the bottom surface as described above, the mechanism of which is perceived to result in a dip in the temperature profile, it is then believed that no significant amount of jet fluid is injected back into the chamber in case P0.92 owing to the lack of the same kind of dip observed in the profile of case P0.84.

Further closing of the end wall in case P0.76, a 3h closing – the size of which is comparable to the nominal jet width, results in a similar flow scenario as described in case P0.84. Beyond this, i.e., the closing s of comparable or larger in size to the jet width δ, the flow is not expected to change its characteristics considerably. Thus, similar or almost the same flow scenario is expected for case P0.76 and cases of more closing. This should explain the similarity in the characteristics of temperature distribution in all the cases with the end opening smaller than that of case P0.76.

5. Conclusions

From the results, we conclude that the change in width of the end-wall closing s has significant impact on the distribution of temperature in the ventilated chamber only in the regime of $s <\sim \delta$; in the other regime, i.e., $s > \delta$, it has almost no effect.

This result has significant implication and application in terms of flow control in a ventilated chamber. For example, one can easily think of a scenario in which effective ventilation is required for a semi-open chamber: to get rid of smell, of exhaust gas, etc. Further investigations concerning effective flow control in ventilated chamber are ongoing.

Finally, it is noted that the supply-air velocity in this study is relatively high such that the wall jet can reach the end wall with some amount of momentum. The scenario is expected to be different for the opposite case.

Acknowledgements

The authors would like to thank all the FMRL graduate members: Mr.'s Kiattisak Kobkanjanakorn, Alongkorn Pimpin, Suthichock Nunthasookkasame, Parama Phromsuthirak, Weerin Wangjiraniran, Pongput Uppathamnarakorn, and Sumeth Tripopsakul, for their assistance in the experiments.

References

1. Gosman, A. D., Nielsen, P. V., Restivo, A., and Whitelaw, J. H., (1980), "The flow properties of rooms with small ventilation openings," *J. Fluids Engineering*, Vol. 102, pp. 316-323.
2. Nielsen, P. V., Restivo, A., and Whitelaw, J. H., (1978), "The velocity characteristics of ventilated rooms," *J. Fluids Engineering*, Vol. 100, pp. 291-298.
3. Peng, S.-H., Davidson, L., and Holmberg, S., (1997), "A modified low-Reynolds number k-ω model for recirculating flows," *J. Fluids Engineering*, Vol. 119, pp. 867-875.
4. Sakulyanontvittaya, T., Ngow, P., Prasartkarnkha, A., Chalokepunrat, S., Pimpin, A., and Bunyajitradulya, A., (1999), "The Design and Development of The FMRL 60x18 cm^2 Wide-Angle Screened-Diffuser Blower Tunnel Part III: The Settling Chamber, The Contraction, and The Wind Tunnel," Proceeding of the 13th National Mechanical Engineering Conference, 2-3 December 1999, Royal Cliff Beach Resort Hotel, South Pattaya, Cholburi.
5. Sathapornnanon, S., Wattanawanichakorn, A., Trakulmaipol, S., Lumluksanapaiboon, M., Pimpin, A., and Bunyajitradulya, A., (1999), "The Design and Development of The FMRL 60x18 cm^2 Wide-Angle Screened-Diffuser Blower Tunnel. Part II: The Screened Diffuser," *Proceeding of the 13th National Mechanical Engineering Conference*, 2-3 December 1999, Royal Cliff Beach Resort Hotel, South Pattaya, Cholburi.

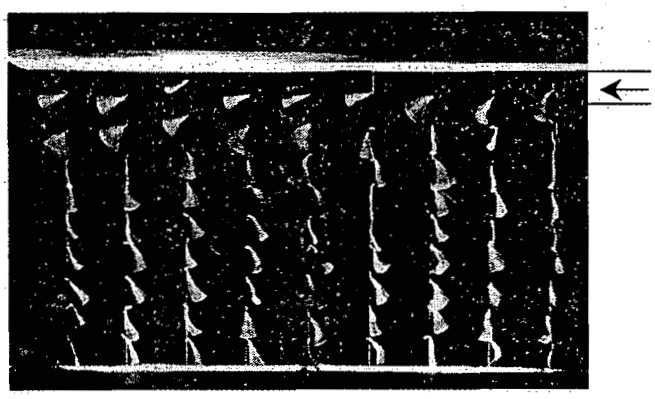

(a) Case P1.0: shutter speed 8 sec.

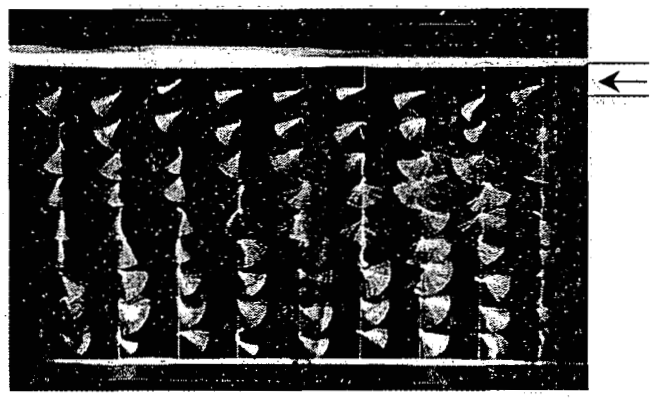

(b) Case P0.76: shutter speed 8 sec.

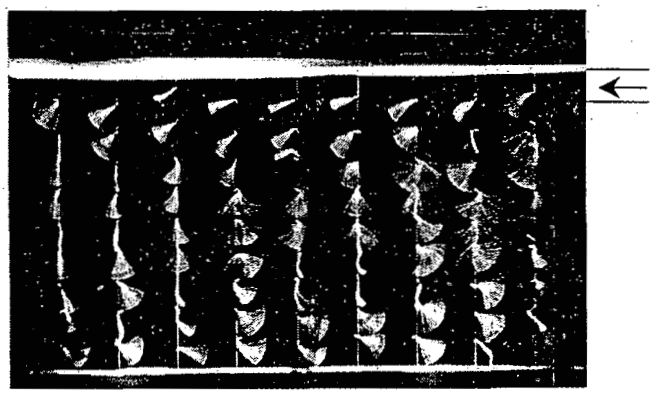

(c) Case P0.08: shutter speed 8 sec.

Fig. 3. Tuft-grid visualizations of cases P1.0, P0.76, and P0.08. Flows are from right to left with the chamber inlet at the top-right corner. The field of view of the images covers the whole chamber.

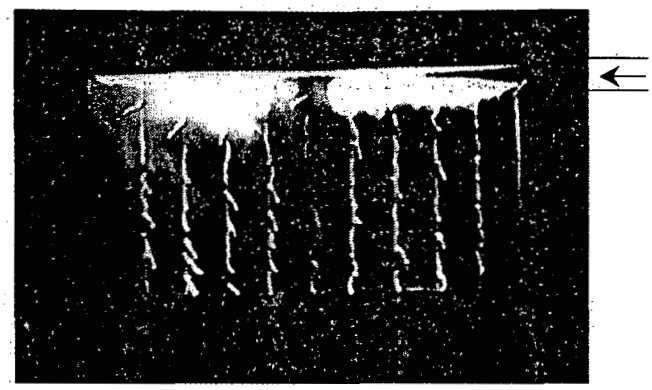

(a) Case P1.0.

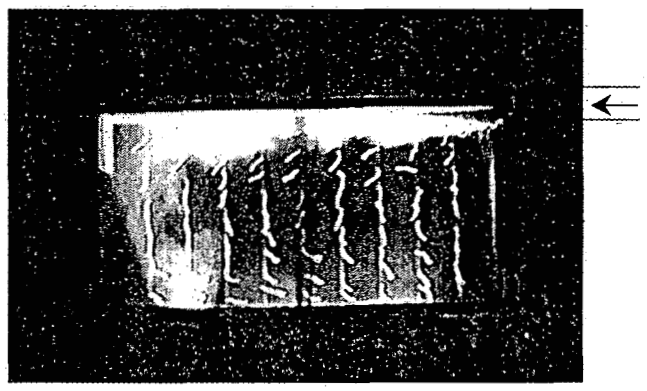

(b) Case P0.76.

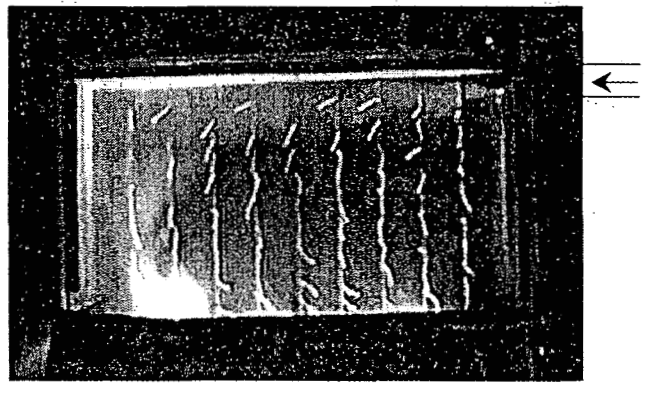

(c) Case P0.08.

Fig. 4. The corresponding powder-injection images of cases in Fig. 3.

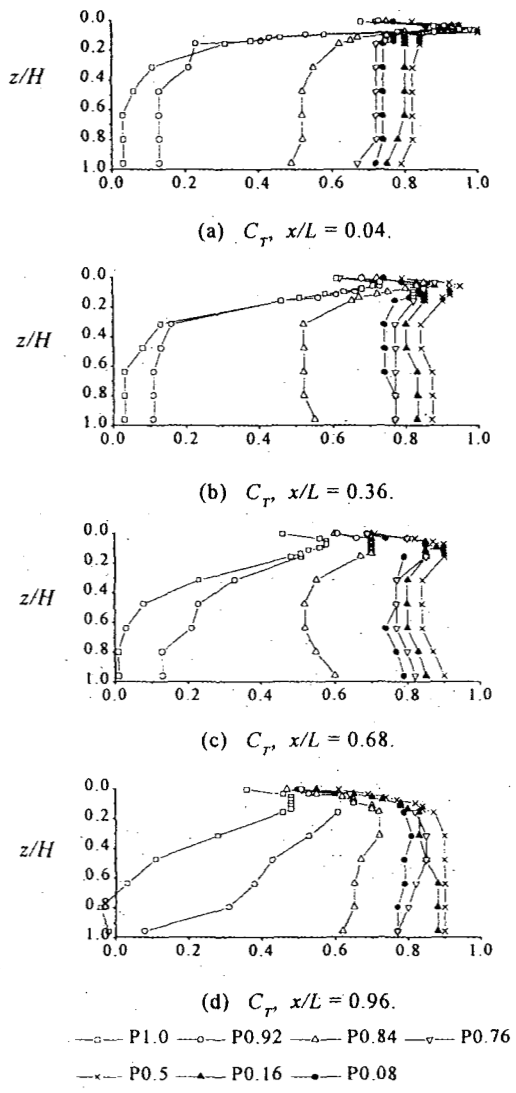

Fig. 5. Effect of end-opening size on temperature distribution on the center plane (y=0).

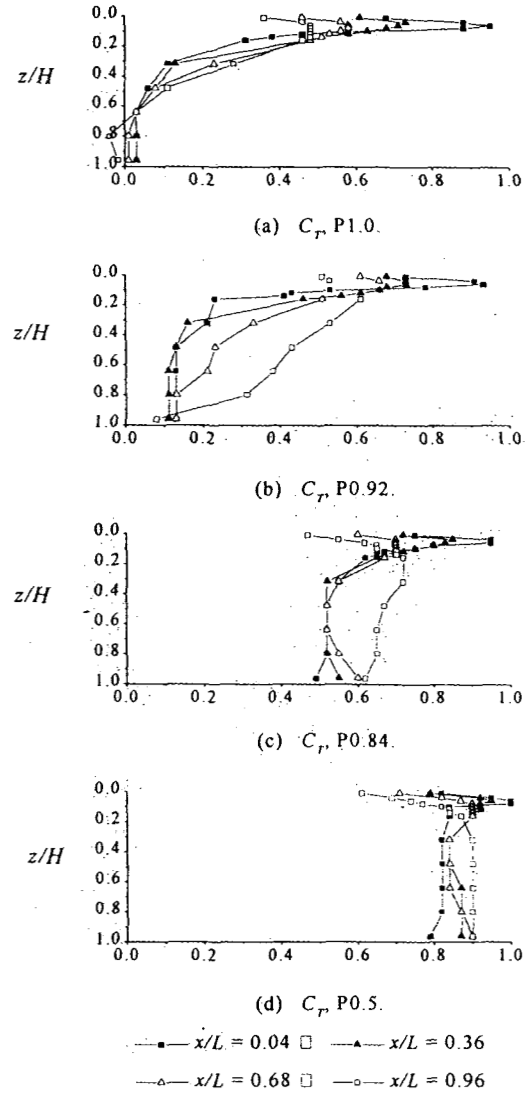

Fig. 6. Temperature distributions for cases P1.0, P0.92, P0.84, and P0.5.

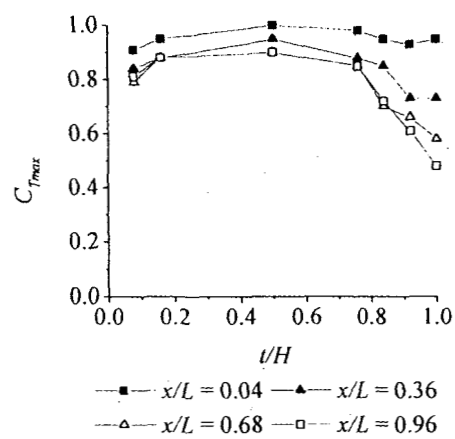

Fig. 7. Effect of end-opening on $C_{T\max}$.

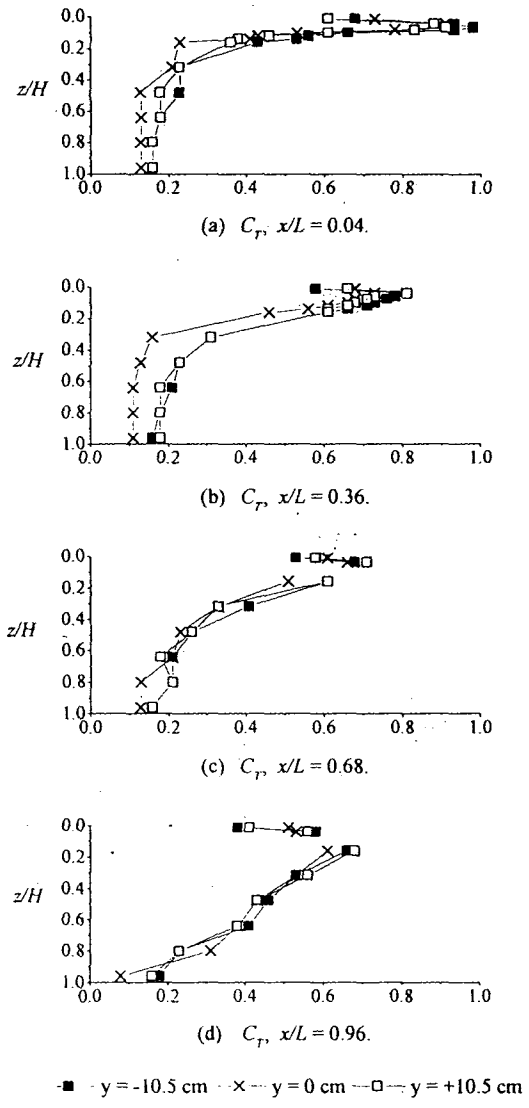

Fig. 8. Temperature distributions along three spanwise planes for case P0.92.